



AIAA 97-2255

**Applications of a Highly Efficient Numerical
Method for Overset-Mesh Moving
Body Problems**

R. H. Nichols

Sverdrup Technology, Inc., AEDC Group
Arnold Engineering Development Center
Arnold Air Force Base, Tennessee 37389
and

R. W. Tramel

Micro Craft, Inc.

Tullahoma, TN 37388

19980608 108

**15th Applied Aerodynamics
Conference**

June 23 - 25, 1997 / Atlanta, GA

For permission to copy or republish, contact the American Institute of Aeronautics and Astronautics
1801 Alexander Bell Drive, Suite 500, Reston, VA 22091

DISTRIBUTION STATEMENT A

Approved for public release;
Distribution Unlimited

DTIC QUALITY INSPECTED 3

APPLICATIONS OF A HIGHLY EFFICIENT NUMERICAL METHOD FOR OVERSET-MESH MOVING BODY PROBLEMS*

*R. H. Nichols***
Sverdrup Technology, Inc., AEDC Group
Arnold Engineering Development Center
Arnold Air Force Base, TN 37389

R. W. Trame†
Micro Craft, Inc.
Tullahoma, TN 37388

Abstract

Several improvements have been incorporated into the XAIR overset-mesh flow solver which substantially improve the capability of the code to perform time-accurate solutions. These improvements include implementing an upwind flux formulation combined with a quasi-Newton relaxation time-stepping strategy. The code includes a very stable $k-\epsilon$ turbulence model which can be used with or without wall function boundary conditions. Results are presented for two moving body cases and two unsteady flows. The new code has demonstrated reductions of CPU times over traditional alternating direction implicit (ADI) methods by factors of 10 for inviscid flows and by orders of magnitude for viscous flows.

Introduction

In order to efficiently compute the trajectories of several bodies moving with mutual aerodynamic influence, a flow solver must be capable of taking very large computational time steps (i.e., running with very large Courant numbers). This demand is especially true when turbulent flows at flight Reynolds numbers are computed. The time step one would like to take in such should be dictated by considerations of numerical accuracy rather than numerical stability. When an overlapping mesh¹ strategy is used, the solutions on each mesh must be tightly coupled in order to assure that the effects of the mutual aerodynamic influence are properly communicated across the interpolated domain boundaries. With this in mind, an effort sponsored by Dr. Leonidas Sakell of the Air Force Office of Scientific Research (AFOSR) was initiated at the Arnold Engineering Development Center (AEDC) to develop the computational tools necessary to simu-

late the ripple launch of three MK-82 stores carried in tandem from an F-15E aircraft at flight Reynolds numbers within a time frame of a few calendar weeks. This requires the solution of the Navier-Stokes equations with a higher-order turbulence model since the aft two stores are immersed in the wake of the store or stores in front of them. Initial estimates of the CPU time requirements for this problem using the existing XAIR² overset-mesh flow solver indicated that calendar years would be required to obtain a solution for the viscous ripple launch. Hence, an effort was made to improve the efficiency, accuracy, and numerical stability of the XAIR² overset-mesh flow solver. This paper presents several applications of the improved code to complex aerodynamic configurations.

Code Improvements

The first improvement to the XAIR code consisted of replacing the central difference flux formulation with the upwind Harten/Lax/van Leer/Einfeldt (HLLC) scheme.^{3,4} The HLLC scheme is an approximate Godunov scheme similar in resolution to Roe's⁵ flux difference scheme. The HLLC scheme was chosen over the Roe scheme because of its lower operation count and because it allows for more direct control of the anti-diffusion terms which are present in both schemes. The latter property is desirable when dealing with the carbuncle phenomena associated with both schemes in hypersonic shock capturing-applications. The HLLC scheme, like the Roe scheme, captures shocks crisply and has very little numerical diffusion in boundary layers. This makes these upwind schemes more accurate than traditional central difference schemes with added second- and fourth-order numerical smoothing. Higher-order spatial accuracy is achieved by using the Monotone

* The research reported herein was performed by the Arnold Engineering Development Center (AEDC), Air Force Materiel Command. Work and analysis for this research were performed by personnel of Sverdrup Technology, Inc., AEDC Group, technical services contractor for AEDC. Further reproduction is authorized to satisfy needs of the U. S. Government.

** Senior Member, AIAA.

† Member, AIAA

This paper is declared a work of the U. S. government and not subject to copyright protection in the United States.

Approved for public release; distribution unlimited.

Upstream Scalar Conservation Law (MUSCL) approach of van Leer.⁶

The second improvement involved replacing the first-order accurate in time Beam and Warming⁷ alternating direction implicit (ADI) scheme with a second-order accurate in time quasi-Newton approach. The Steger-Warming flux linearizations are used to approximate the inviscid part of the flux Jacobians required by the Newton method. As shown by Whitfield, et al.⁸, the use of Steger-Warming linearizations provides the numerical stability required to take large time steps. The viscous part of the Newton flux Jacobians is provided by linearizing the thin-layer viscous fluxes. Source term Jacobian contributions for the $k-\epsilon$ ⁹ and Spalart-Allmaras¹⁰ turbulence models are provided by approximations of the linearized source terms. The tridiagonal system of linear equations which must be solved at each iteration of the Newton process is treated using the Jacobi iterative method^{11,12} with underrelaxation. Second-order time accuracy is achieved by using three-point backward differencing.

All computational boundaries within the computational domain are updated within the Newton loop. This causes explicitly applied boundary conditions to behave in a pseudo-implicit manner. Thus, at the completion of each time step, the flow variables at the boundaries are at the same time level as the interior points. Periodic boundaries such as slits (C-mesh topology), overlaps (O-mesh topology), and symmetry planes are treated implicitly through the introduction of ghost cells. This eliminates the "ringing" at these boundaries often encountered with explicit periodic boundary conditions and allows the use of higher-order fluxes at these boundaries. Global coupling between the overlapping grids is also handled within the Newton loop, so that at the end of each time step the entire computational domain has advanced to the same time level.

The turbulence models ($k-\epsilon$ ⁹ and Spalart-Allmaras¹⁰) are also included within the Newton loop. The Newton methodology thus provides a pseudo-coupling of the turbulence equations to the mean flow equations. The wall function boundary conditions of Nichols⁹ are available for both turbulence models.

These improvements to the XAIR code have substantially increased the allowable time step which the flow solver can take. The new code has demonstrated the ability to take time steps 10-20 times larger than its predecessor for inviscid calculations, and is capable of orders of magnitude improvements for viscous flow. Local time stepping is not required for numerical stability with the new code, so all problems may be treated as time-accurate calculations. This has provided insight in several applications at AEDC which would not have been available with a code which requires local time stepping. More details on the new code can be found in Ref. 13.

Applications

Three unsteady and two moving body problems are presented which demonstrate the capabilities of the new flow solver. The unsteady test cases include vortex shedding from a circular cylinder at high Reynolds number, and a simple cavity. The moving body problems are the launch of a single generic store and the ripple launch of three generic stores.

The unsteady cases presented here utilize conventional two-equation turbulence models. The differential equations solved for these turbulence models include the proper unsteady terms, but the question still remains as to how applicable these turbulence models are to unsteady flows. A turbulence model applicable to unsteady flow should be capable of differentiating between unsteady length and time scales and the sub-grid size turbulence. The turbulence model should only try to simulate the effects of the sub-grid turbulence. Conventional one-equation and two-equation turbulence models actually simulate the effect of turbulent scales larger than the computational cell size and provide no mechanism for filtering out the large-scale contribution. Large Eddy Simulation (LES) turbulence models attempt to provide a filter for the turbulent scales, but these models have yet to mature to the point of application for complex three-dimensional flow problems. It is expected that the conventional turbulence models will overpredict the effect of turbulence in unsteady applications and overdamp the unsteady nature of the flow. The amount of this overdamping cannot be accurately determined at this time, and is probably dependent on the formulation of the particular turbulence model.

DTIC QUALITY INSPECTED 3

Vortex Shedding From a Circular Cylinder

The first unsteady flow test case was the flow past a circular cylinder with a free-stream Mach number of 0.2 and a Reynolds number of 8×10^6 based on the diameter of the cylinder. Experimental data for this high Reynolds number condition have been obtained by Jones, et al.¹⁴ and by Roshko.¹⁵ This case was chosen because the flow on the cylinder is almost fully turbulent and a definite vortex shedding frequency is present. Jones, et al.¹⁴, identify three regimes for high Reynolds number flow over a circular cylinder ($Re > 1 \times 10^6$) in terms of the Strouhal number (St):

$1.0 \times 10^6 < Re < 3.5 \times 10^6$ Wide band unsteady lift force (wide St bandwidth)

$3.5 \times 10^6 < Re < 6.0 \times 10^6$ Narrow band random lift forces (narrowing St bandwidth)

$6.0 \times 10^6 < Re < 1.0 \times 10^7$ Quasi-periodic lift forces (small St bandwidth)

Hence it is expected that the lift force on the cylinder will oscillate at a predominant frequency for this test case. Unfortunately, the available data also indicate a sudden drag rise near this condition, and large variations in the drag coefficient are reported. The pressure taps used by Jones, et al.¹⁴ were located only one cylinder diameter from the tunnel floor. Flow visualization results indicate some three dimensionality was indeed present in the experiment. The data of Roshko¹⁵ were taken in a solid wall tunnel with a model blockage (the ratio of model frontal area to tunnel cross-sectional area) of about 19 percent. A 10-percent reduction was made in the drag coefficient to correct the data for wall effects, but the author admits that the corrections have questionable validity at these conditions for unsteady force measurements. The data of Jones, et al.¹⁴ were taken in a slotted wall tunnel, and also had a model blockage of about 19 percent. No wall corrections were made for the data. The cylinder used by Jones had a smoother surface than did the model of Roshko. The large model blockage may contribute to the large variation in reported drag coefficients. It would be expected that wall interference would cause the flow to over-accelerate at the top and bottom of the cylinder. This would cause a reduction in the pressure in the

suction peak and probably delay flow separation. These two effects would cause the base pressure to drop, and hence lead to a larger value of drag. Thus, one would expect the drag coefficient reported by Roshko¹⁵ to be larger than that of Jones, et al.¹⁴, and that both would be larger than an interference-free result as calculated here. As will be seen, this is the case. The Strouhal number reported by both investigations is in reasonable agreement. Hence, the ability to predict the Strouhal number will be used as one metric for evaluating the code.

Calculations were performed with a 401×201 grid with an initial y^+ of 50 using the $k-\epsilon$ turbulence model with wall function boundary conditions, and with a 401×211 grid with an initial y^+ of 1 using the low Reynolds number $k-\epsilon$ turbulence model (integrating the turbulence equations to the wall). A physical time step of 4.3×10^{-4} secs was used for both grids, resulting in a maximum Courant number of 4770 for the wall function grid and a Courant number of 2.32×10^5 for the low Reynolds number grid. The calculations were begun from uniform free-stream conditions. A periodic condition was reached after about 1,000 iterations, and the solution was advanced another 2,048 steps to provide averaged results.

Figure 1 shows the Mach number contours at a particular instant in time. The periodic disturbance is seen to dissipate as it moves downstream until a steady wake is finally achieved. Unfortunately, there are no experimental data available with which to compare the disturbance dissipation distance. It is interesting to note that Roshko¹⁵ made hot-wire measurements seven diameters behind the cylinder and noted unsteady flow still present. The

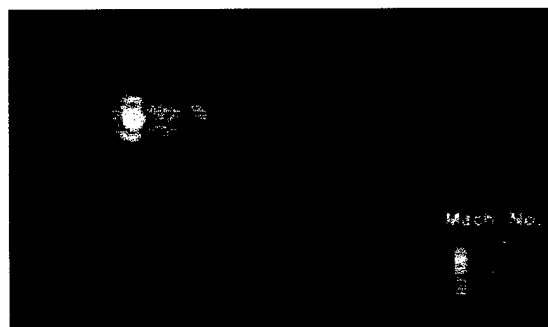


Fig. 1. Mach number contours for a circular cylinder at $M = 0.2$ and $Re = 8 \times 10^6$.

results presented still show unsteady flow seven diameters behind the cylinder. Roshko also reported no unsteady flow was present at this location when the Reynolds number was reduced to around 1×10^6 . In an earlier study, Delaney and Sorenson¹⁶ discovered unsteady flow at a Reynolds number of 1×10^6 using a hot wire located two diameters behind the cylinder. Hence, it seems that the unsteady flow dissipates rapidly at these high Reynolds numbers and the length over which this dissipation occurs is Reynolds number dependent. Detailed data on the dissipation distance for the cylinder unsteady wake would be useful in evaluating turbulence models for unsteady flow applications.

The computational and experimental average drag coefficient and the unsteady lift coefficient Strouhal number are shown in Table 1. The average drag coefficient is underpredicted by CFD, which may be attributable to either an overprediction of the base pressure or a premature prediction of the boundary-layer separation point. As explained above, the results are consistent with the amount of wall interference present in the experimental and computational studies. The Strouhal number predictions are in reasonable agreement. The spectrum of the CFD results is shown in Fig. 2. More than 90 percent of the energy is seen to be concentrated in the first spectral peak, indicating a truly periodic result.

Cavity

A single computation using the wall function boundary condition in conjunction with the $k-\epsilon$ turbulence model was performed for a three-dimensional cavity. The cavity had a length-to-depth ratio of 4.5. The flow computations were performed for a free-stream Mach number of 1.2 and a Reynolds number of 2.0×10^6 per foot. The characteristic time, t_c (the time required for free-stream flow to

Table 1. Computational and Experimental Results for a Circular Cylinder at $M = 0.2$ and $Re = 8 \times 10^6$

	Average Cd	Strouhal Number
Wall Function CFD	0.382	0.293
Low Reynolds Number $k-\epsilon$ CFD	0.425	0.273
Data Jones et al. ¹⁴	0.50-0.55	0.29-0.31
Data Roshko et al. ¹⁵	0.68-0.75	0.27

traverse the cavity), is 0.00144 secs. Data used for comparisons were obtained during the Weapons Internal Carriage Separation Program (WICS) sponsored by the Wright Laboratory/Armament Directorate.¹⁷ The basic configuration tested, shown in Fig. 3, was a generic flat plate and cavity. Both static and dynamic pressure data were obtained during the test.

A coarse grid of approximately 2×10^5 points was used to model half of the bay and flat plate. A time step of 8×10^{-5} seconds was used for the calculations. The time step is approximately 50 times

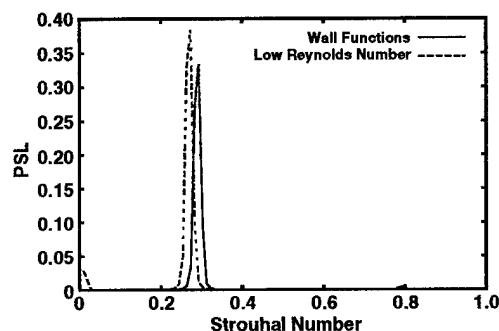


Fig. 2. Spectrum of the normal force coefficient predictions for a cylinder at $M = 0.2$ and $Re = 8 \times 10^6$.

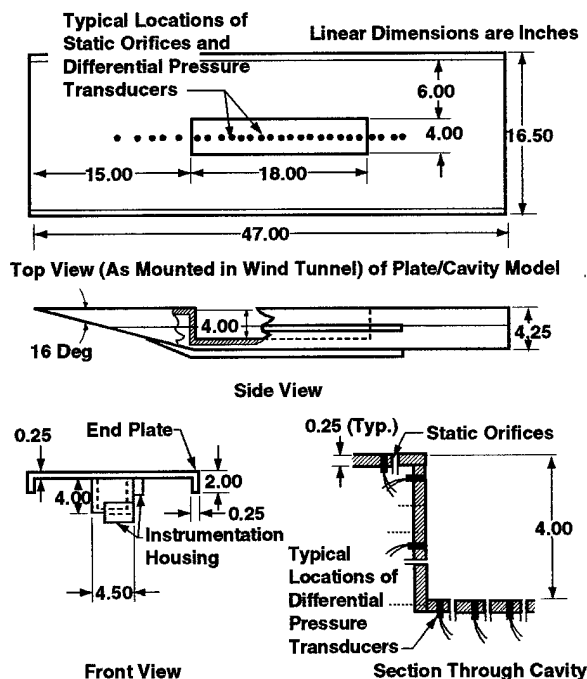


Fig. 3. Dimensions of the WICS flat-plate/cavity model.

larger than the time step used to calculate this flow by Suhs, et al.¹⁸ using the Ref. 2 flow solver with the same turbulence model and wall function boundary conditions. The calculated instantaneous pressure on the back wall of the cavity is shown in Fig. 4. The transients due to the initial conditions are seen to disappear after approximately 20 time characteristics, after which the flow is periodic. About 0.01 secs of computational data taken after

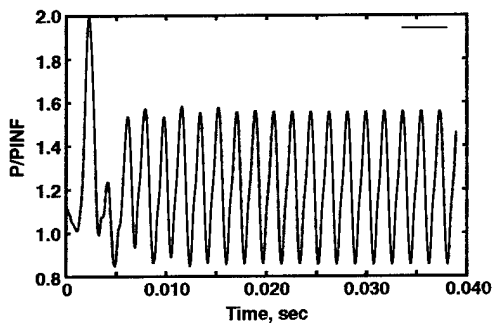
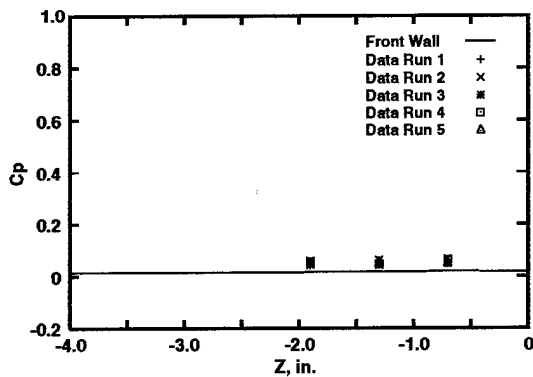


Fig. 4. Predicted pressure on the aft wall of the WIC bay.

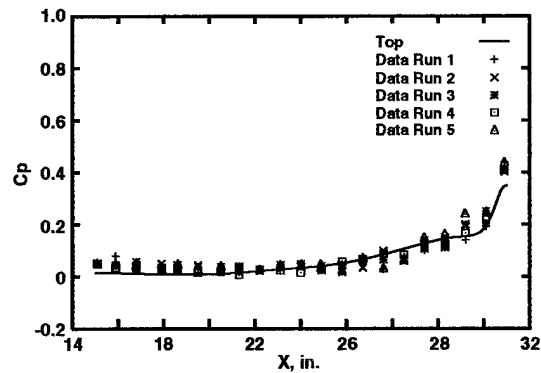
the flow had become periodic was used to provide time-averaged and spectral data for the weapons bay. The averaged pressure coefficients on the bay centerline are shown, along with experimental data in Fig. 5. The computed and experimental sound pressure levels are shown in Fig. 6. The agreement is good for both of these quantities and consistent with Suhs' results. The spectrum for a point on the centerline of the bay back wall is shown in Fig. 7, along with the first two experimental spectral peaks. It should be noted that the background noise sound pressure level generated by the holes of the porous wind tunnel walls is about 120 dB. Again, the agreement is quite good. For this case, the total savings in CPU time using the new solution algorithm was a factor of ten over that of the ADI scheme.

Generic Store Release

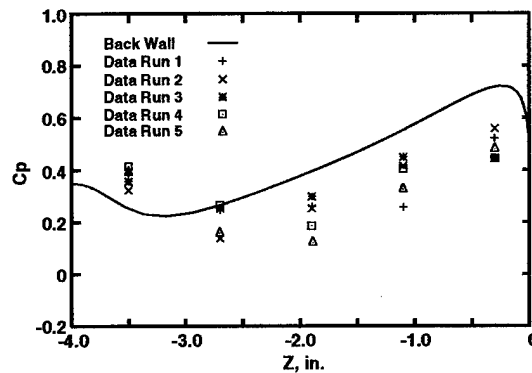
The first moving body case chosen for presentation is the generic wing/pylon/finned store configuration



a. Front wall



b. Bottom wall



c. Back wall

Fig. 5. Time-averaged pressure coefficient for the WICS bay centerline.

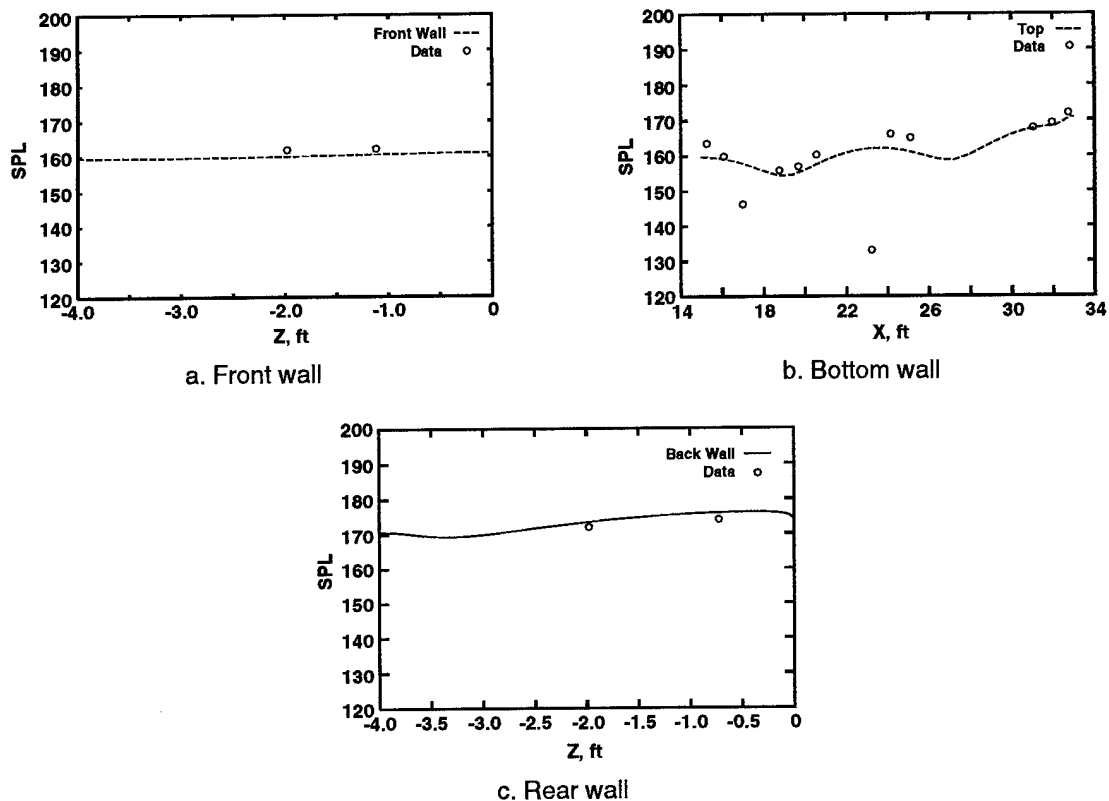


Fig. 6. Sound pressure level for the WICS bay centerline.

ration.¹⁹ The store physical properties and ejector forces are given in Ref. 19. Euler calculations were performed for a free-stream Mach number of 0.95 on a 1.5×10^6 point grid system. The chimera moving body methodology of Jordan, et al.²⁰ was used to model the store launch. A computational time step of 0.00165 secs was used with the new code, resulting in a maximum Courant number of 4000 for the grid system. This time step is 16 times larger than that used by previous investigators.^{19,21} The predicted carriage loads are presented in Table 2. The pressure coefficient distribution for the store at carriage is shown in Fig. 8. Results of the computed and experimental trajectories are shown in Figs. 9-12. In all cases, the agreement is excellent. The results are consistent with those of Lijewski¹⁹ and Thoms and Jordan.²¹ For this case, the total savings in CPU time was a factor of six over that reported by Thoms and Jordan.²¹

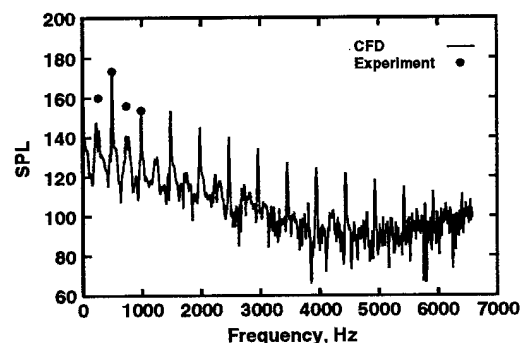


Fig. 7. Spectrum of the sound pressure level on the back wall of the WICS bay.

Table 2. Predicted and Measured Carriage Loads for the Single Generic Store

	CA	CY	CN	CI	Cm	Cn
Lijewski ¹⁹	0.74	-1.08	0.73	0.10	-1.69	1.88
Thoms ²¹	0.90	-1.09	0.69	0.10	-1.73	1.84
Present	0.92	-1.01	0.63	0.09	-1.58	1.62
Exp. ¹⁹	0.901 ± 0.053	-0.954 ± 0.035	0.664 ± 0.057	0.1 ± 0.058	-1.43 ± 0.10	1.52 ± 0.056

TER Ripple Launch

The final case presented is a multiple-body release from a triple ejector rack (TER) configuration. The case included the wing/pylon configuration from the previous test case, along with three generic stores. The store physical properties and

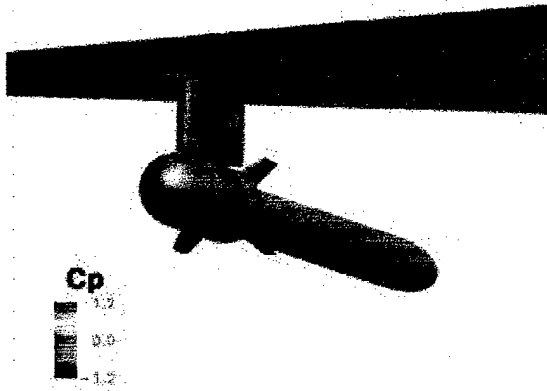


Fig. 8. Pressure coefficient contours on the generic store at carriage.

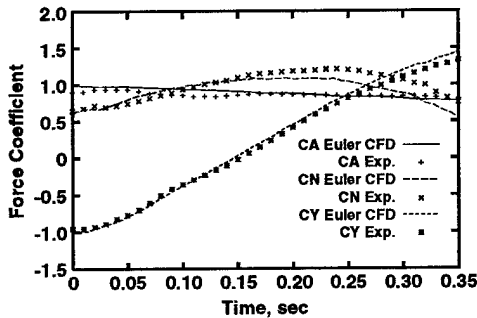


Fig. 9. Comparison of computed and measured force coefficients for the single generic store.

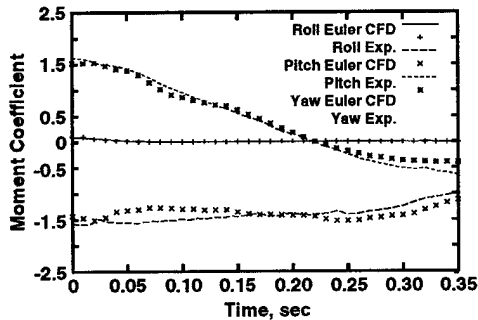


Fig. 10. Comparison of computed and measured moment coefficients for the single generic store.

ejector forces are given in Ref. 21. The bottom store was released first at $t = 0.000$ sec, followed by the outboard store at $t = 0.040$ sec, and finally the inboard store at $t = 0.080$ sec. The grid system included 3.2×10^6 points. The flight condition selected for this demonstration was a free-stream Mach number of 0.95 and an altitude of 20,000 ft. The $k-\epsilon$ turbulence model was used, along with the wall function boundary conditions. The computations were performed using a time step of 0.0033 secs, which is a factor of 32 times larger than the time step used in the Euler calculations of Thoms and Jordan.²¹ The maximum Courant number was 1×10^4 . Pressure coefficient distributions with the stores at carriage are shown in Fig. 13. The predicted carriage loads are shown in Table 3. The present viscous loads are generally smaller than the Euler results of Thoms and Jordan.²¹ This is consistent with the forward movement of the shock in the tail region of the stores due to thickening and separation of the boundary layer. The computational predictions for the inboard, outboard, and bottom store trajectories and Euler angles are

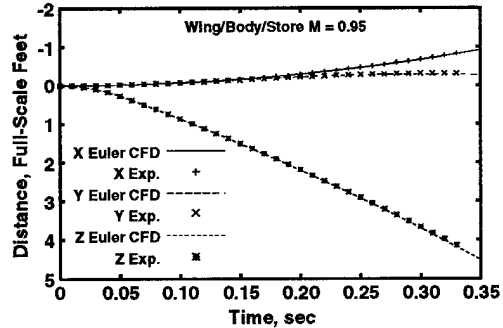


Fig. 11. Comparison of computed and measured store trajectory for the single generic store.

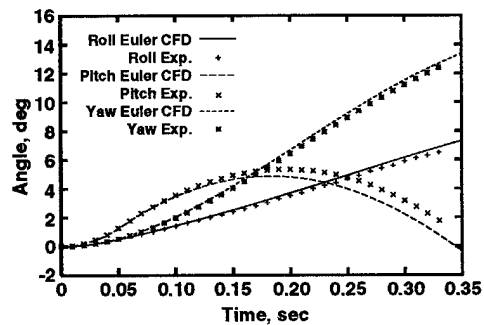


Fig. 12. Comparison of computed and measured store orientation for the single generic store.

shown in Figs. 14-19. The predicted roll angle for the bottom store at the end of the trajectory is about three times larger than that predicted by Thoms and Jordan.²¹ The predicted roll angle of the inboard and outboard stores is opposite of that predicted by Thoms and Jordan.²¹ The pitch angle results are similar between the two predictions as expected since they are dominated by the ejectors. It should be noted that the present Navier-Stokes calculations required one-third of the CPU time required for the Euler predictions of Thoms and Jordan.²¹

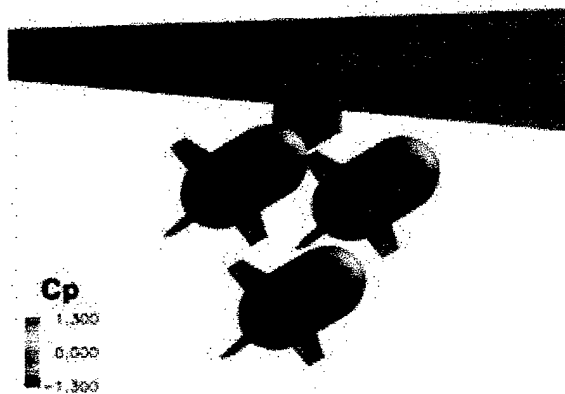


Fig. 13. Pressure coefficient contours on three generic stores at in TER configuration.

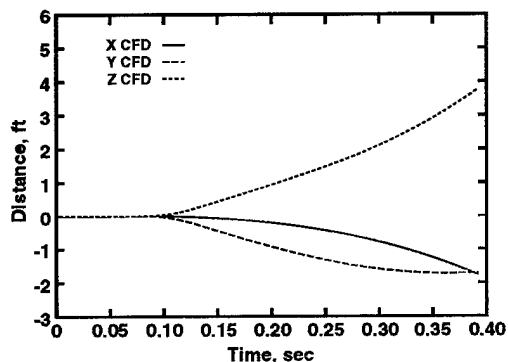


Fig. 14. TER inboard store trajectory.

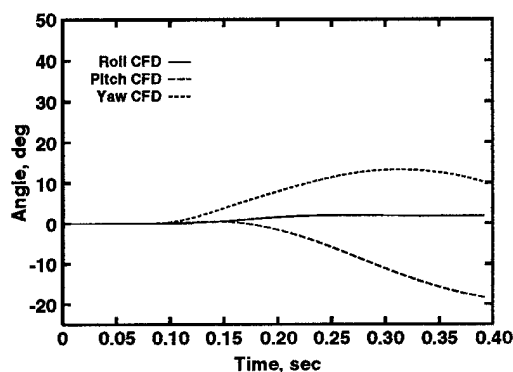


Fig. 15. TER inboard store orientation.

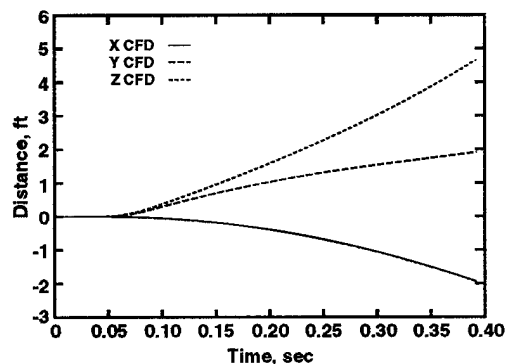


Fig. 16. TER outboard store trajectory.

Table 3. Predicted Carriage Loads for the Stores in a TER Configuration

	CA	CY	CN	Cl	Cm	Cn
Bottom Store Thoms ²¹	1.134	-0.266	0.286	0.001	-0.869	0.535
Bottom Store Present	0.974	-0.243	0.137	-0.023	-0.532	0.537
Inner Store Thoms ²¹	1.382	-0.704	1.093	-0.060	-2.999	1.094
Inner Store Present	0.945	-0.626	0.709	0.007	-2.047	0.828
Outer Store Thoms ²¹	1.180	-0.432	0.118	-0.010	-1.001	0.911
Outer Present	1.007	-0.313	-0.052	-0.004	-0.723	0.789

Conclusions

Several improvements have been incorporated into the XAIR overset mesh flow solver which substantially improve the capability of the code to perform time-accurate solutions. These improvements include implementing an upwind flux formulation combined with a quasi-Newton relaxation time-stepping strategy. In addition, use is made of the wall function boundary condition for both the Spalart-Allmaras and $k-\epsilon$ turbulence models to reduce the number of grid points in the boundary layer and to reduce the maximum Courant number occurring in a computational mesh. The new code

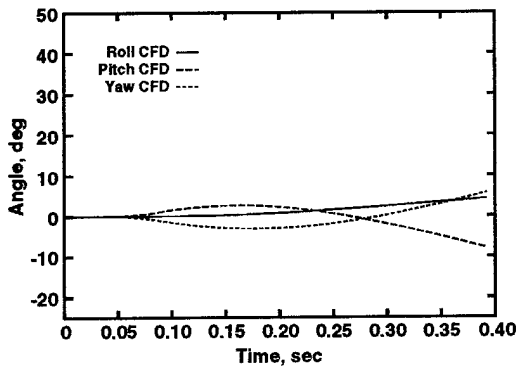


Fig. 17. TER outboard store orientation.

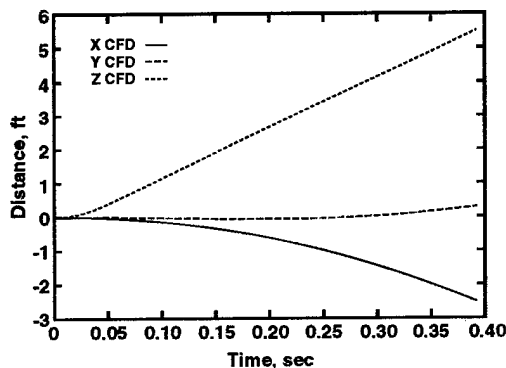


Fig. 18. TER bottom store trajectory.

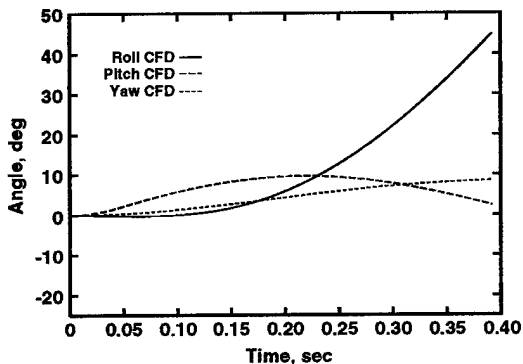


Fig. 16. TER bottom store orientation.

has been tested on a variety of steady and unsteady flows. Four of these test cases are presented. The improvements have allowed computations to be performed with time steps ten times larger than previous ADI methods for Euler flows, and has increased the maximum time step by orders of magnitude for viscous flows. Further validation efforts are underway and will be reported at a later date.

References

1. Benek, J. A., Steger, J. L., Dougherty, F. C., and Buning, P. G. "Chimera: A Grid-Embedding Technique." AEDC-TR-85-64 (AD-A167466), December 1985.

2. Benek, J. A., Donegan, T. L., and Suhs, N. E. "Extended Chimera Grid Embedding Scheme with Application to Viscous Flows." AIAA-87-1126-CP, June 1987.

3. Einfeldt, B. "On Godunov-Type Methods for Gas Dynamics." *SIAM Journal of Numerical Analysis*, Vol. 25, No. 2, April 1988, pp. 294-318.

4. Einfeldt, B., Munz, C. D., Roe, P. L., and Sjogreen, B. "On Godunov-Type Methods Near Low Densities." *Journal of Computational Physics*, Vol. 92, No. 2, 1991, pp. 273-295.

5. Roe, P. L. "Approximate Riemann Solvers, Parameter Vectors, and Difference Schemes." *Journal of Computational Physics*, Vol. 53, 1981, pp. 357-372.

6. van Leer, B. "Towards the Ultimate Conservative Difference Scheme V. A Second Sequel to Godunov's Method." *Journal of Computational Physics*, Vol. 32, 1979, pp. 101-136.

7. Beam, R. F. and Warming, R. "On the Construction and Application of Implicit Factored Schemes for Conservation Laws." SIAM-AMS Proceedings, Vol. 11, Proceedings of the Symposium on Computational Fluid Mechanics, New York, 1977.

8. Whitfield, D. L., Janus, J. M., and Simpson, L. B. "Implicit Finite Volume High Resolution Wave-Split Scheme for Solving the Unsteady Three-Dimensional Euler and Navier-Stokes Equations on Stationary or Dynamic Grids." Engineering and Industrial Research Station Report MSSU-EIRS-ASE-88-2, Mississippi State University, Mississippi State, MS, February 1988.

9. Nichols, R.H. "Development and Validation of a Two-Equation Turbulence Model with Wall Functions for Compressible Flow." AIAA-96-2385, June 1996.

10. Spalart, P. R. and Allmaras, S. R. "A One Equation Turbulence Model for Aerodynamic Flows." AIAA-92-0439, January 1992.
11. Young, D. M. *Iterative Solution of Large Linear Systems*. Academic Press, Inc., New York, 1971.
12. Wright, M. J., Candler, G. V., and Prampolini, M. "Data-Parallel Lower-Upper Relaxation Method for the Navier-Stokes Equations." *AIAA Journal*, Vol. 34, No. 7, July 1996, pp. 1371-1377.
13. Tramel, R. W. and Nichols, R. H. "A Highly-Efficient Numerical Method for Overset-Mesh Moving-Body Problems." AIAA-97-2040, July 1997.
14. Jones, G. W., Cincotta, J. J., and Walker, R. W. "Aerodynamic Forces on a Stationary and Oscillating Circular Cylinder at High Reynolds Numbers." NASA-TR-R-300, October 1968.
15. Roshko, A. "Experiments on the Flow Past a Circular Cylinder at Very High Reynolds Number." *Journal of Fluid Mechanics*, Vol. 10, Part 3, May 1961, pp. 345-356.
16. Delaney, N. K. and Sorensoen, N. E. "Low Speed Drag of Cylinders of Various Shapes." NACA TN 3038, 1953.
17. Dix, R. E. and Butler, C. "Cavity Aeroacoustics." Proceedings of Store Carriage, Integration and Release Conference, Bath, U.K., The Royal Aeronautical Society, April 1990.
18. Suhs, N. E., Nichols, R. H., and Denny, A. G. "Unsteady Viscous Flow Computations Using a Two-Equation Turbulence Model with Wall Functions." AIAA-96-2430, July 1996.
19. Lijewski, L. and Suhs, N. E. "Chimera-Eagle Store Separation." AIAA-92-4569, August 1992.
20. Jordan, J. K., Suhs, N. E., Thoms, R. E., Tramel, R. W., Fox, J. H., and Erickson, J. C., Jr. "Computational Time Accurate Body Movement: Methodology, Validation, and Application." AEDC-TR-94-15, October 1995.
21. Thoms, R. D. and Jordan, J. K. "Investigation of Multiple-Body Trajectory Prediction Using Time-Accurate Computational Fluid Dynamics." AIAA-95-1870, June 1995.

REPORT DOCUMENTATION PAGE			Form Approved OMB No. 0704-0188	
Public reporting burden for this collection of information is estimated to average 1 hour per response, including the time for reviewing instructions, searching existing data sources, gathering and maintaining the data needed, and completing and reviewing the collection of information. Send comments regarding this burden estimate or any other aspect of this collection of information, including suggestions for reducing this burden, to Washington Headquarters Services, Directorate for Information Operations and Reports, 1215 Jefferson Davis Highway, Suite 1204, Arlington, VA 22202-4302, and to the Office of Management and Budget, Paperwork Reduction Project (0704-0188), Washington, DC 20503.				
1. AGENCY USE ONLY (Leave blank)	2. REPORT DATE June 1997	3. REPORT TYPE AND DATES COVERED Technical Society Paper		
4. TITLE AND SUBTITLE Applications of a Highly Efficient Numerical Method for Overset-Mesh Moving Body Problems AIAA Paper No. 97-2255			5. FUNDING NUMBERS	
6. AUTHOR(S) R. W. Tramel and R. H. Nichols				
7. PERFORMING ORGANIZATION NAME(S) AND ADDRESS(ES) Sverdrup Technology, Inc./AEDC Group 740 Fourth Street Arnold Air Force Base, Tennessee 37389-6001			8. PERFORMING ORGANIZATION REPORT NUMBER	
9. SPONSORING/MONITORING AGENCY NAME(S) AND ADDRESS(ES) Arnold Engineering Development Center Arnold AFB, TN 37389			10. SPONSORING/MONITORING AGENCY REPORT NUMBER	
11. SUPPLEMENTARY NOTES 15th AIAA Applied Aerodynamics Conference, Snowmass, CO, June 29-July 2, 1997				
12a. DISTRIBUTION AVAILABILITY STATEMENT Approved for public release; distribution unlimited.			12b. DISTRIBUTION CODE A	
13. ABSTRACT (Maximum 200 words) Several improvements have been incorporated into the XAIR overset-mesh flow solver which substantially improve the capability of the code to perform time-accurate solutions. These improvements include implementing an upwind flux formulation combined with a quasi-Newton relaxation time-stepping strategy. The code includes a very stable k-e turbulence model which can be used with or without wall function boundary conditions. Results are presented for two moving body cases and two unsteady flows. The new code has demonstrated reductions of CPU times over traditional alternating direction implicit (ADI) methods by factors of 10 for inviscid flows and by orders of magnitude for viscous flows.				
14. SUBJECT TERMS CFD, algorithm, moving body, overset-mesh			15. NUMBER OF PAGES 11	
			16. PRICE CODE	
17. SECURITY CLASSIFICATION OF REPORT Unclassified	18. SECURITY CLASSIFICATION OF THIS PAGE Unclassified	19. SECURITY CLASSIFICATION OF ABSTRACT Unclassified	20. LIMITATION OF ABSTRACT UL	